Relief of the Dma1-mediated checkpoint requires Dma1 autoubiquitination and dynamic localization

Christine M. Jones[†,‡], Jun-Song Chen[†], Alyssa E. Johnson[§], Zachary C. Elmore[‖], Sierra N. Cullati, Janel R. Beckley, and Kathleen L. Gould*
Department of Cell and Developmental Biology, Vanderbilt University School of Medicine, Nashville, TN 37240

ABSTRACT **Chromosome segregation and cell division are coupled to prevent aneuploidy and cell death. In the fission yeast *Schizosaccharomyces pombe*, the septation initiation network (SIN) promotes cytokinesis, but upon mitotic checkpoint activation, the SIN is actively inhibited to prevent cytokinesis from occurring before chromosomes have safely segregated. SIN inhibition during the mitotic checkpoint is mediated by the E3 ubiquitin ligase Dma1. Dma1 binds to the CK1-phosphorylated SIN scaffold protein Sid4 at the spindle pole body (SPB), and ubiquitinates it. Sid4 ubiquitination antagonizes the SPB localization of the Polo-like kinase Plo1, the major SIN activator, so that SIN signaling is delayed. How this checkpoint is silenced once spindle defects are resolved has not been clear. Here we establish that Dma1 transiently leaves SPBs during anaphase B due to extensive autoubiquitination. The SIN is required for Dma1 to return to SPBs later in anaphase. Blocking Dma1 removal from SPBs by permanently tethering it to Sid4 prevents SIN activation and cytokinesis. Therefore, controlling Dma1's SPB dynamics in anaphase is an essential step in *S. pombe* cell division and the silencing of the Dma1-dependent mitotic checkpoint.**

Monitoring Editor
Rong Li
Johns Hopkins University

Received: Apr 27, 2018
Revised: Jun 25, 2018
Accepted: Jun 27, 2018

INTRODUCTION

Accurate cell division, yielding two genetically identical daughter cells, requires coordination between mitosis and cytokinesis. In the fission yeast *Schizosaccharomyces pombe*, the septation initiation network (SIN), a protein kinase cascade, coordinates these two events by initiating cytokinesis after chromosome segregation (for review see Krapp and Simanis, 2008; Johnson *et al.*, 2012b; Simanis, 2015). When there is a mitotic error, a checkpoint mechanism inhibits SIN signaling to prevent cytokinesis from occurring before chromosomes have safely segregated (Marks *et al.*, 1992; Murone and Simanis, 1996; Guertin *et al.*, 2002; Johnson and Gould, 2011). This checkpoint operates in parallel to the spindle assembly checkpoint (Murone and Simanis, 1996; Johnson *et al.*, 2013; Musacchio, 2015). Checkpoints with the similar purpose of maintaining coordination between chromosome segregation and cytokinesis also exist in *Saccharomyces cerevisiae* and mammals (Mendoza and Barral, 2008; Caydasi and Pereira, 2012; Nahse *et al.*, 2017).

SIN inhibition during a mitotic error depends on the dimeric E3 ubiquitin ligase Dma1, a member of the FHA and RING finger family (Brooks *et al.*, 2008). Dma1 was identified as a high copy suppressor of a hyperactive SIN mutant, and it is required to prevent septation during a prometaphase arrest elicited by the ß-tubulin mutant *nda3-km311* (Hiraoka *et al.*, 1984; Murone and Simanis, 1996). Overproduction of Dma1 completely blocks SIN activity and results in cell death (Guertin *et al.*, 2002), indicating its levels and activity must be properly regulated. Dma1 colocalizes with SIN components both at the cell division site and at the mitotic spindle pole body (SPB)

This article was published online ahead of print in MBoC in Press (http://www.molbiolcell.org/cgi/doi/10.1091/mbc.E18-04-0261) on July 5, 2018.

[†]These authors contributed equally to this work.

Present addresses: [‡]Abcam, 688 East Main Street, Branford, CT 06405 (christine.jones@abcam.com); [§]Department of Biological Sciences, Louisiana State University, Baton Rouge, LA 70803 (johnsona@lsu.edu); [‖]Gene Therapy Center, University of North Carolina at Chapel Hill, Chapel Hill, NC 27599 (zachary_elmore@med.unc.edu).

Author contributions: Conception and design of work: C.M.J, J.-S.C., A.E.J., S.N.C., and K.L.G; acquisition of data: C.M.J, J.-S.C., A.E.J., S.N.C., and Z.C.E; analysis and interpretation of data: all authors; writing and editing manuscript: all authors.

The authors declare that they have no conflict of interest.

*Address correspondence to: Kathleen L. Gould (kathy.gould@vanderbilt.edu).

Abbreviations used: CR, contractile ring; GBP, GFP-binding protein; mNG, mNeonGreen; SIN, septation initiation network; SPB, spindle pole body.

(Guertin *et al.*, 2002); however, it is Dma1's SPB localization and its ubiquitination of the SIN scaffold protein, Sid4 (Chang and Gould, 2000; Morrell *et al.*, 2004), that is required for SIN inhibition during a mitotic checkpoint (Johnson and Gould, 2011). Sid4 ubiquitination antagonizes the SPB localization of the Polo-like kinase Plo1 (Guertin *et al.*, 2002; Johnson and Gould, 2011), the major SIN activator (Ohkura *et al.*, 1995; Mulvihill *et al.*, 1999; Tanaka *et al.*, 2001), so that SIN signaling is blocked and cytokinesis is delayed.

Upon resolution of the mitotic spindle defect, the Dma1-dependent checkpoint signal must be extinguished to resume SIN activation and cell division. Here we report that Dma1 exhibits striking fluctuations in its localization to SPBs and the division site during the cell cycle. We found that both SIN activity and Dma1 autoubiquitination modulate Dma1 SPB localization dynamics and therefore its ability to inhibit the SIN. By permanently tethering Dma1 to SPBs and preventing these fluctuations, the SIN fails to become active and cytokinesis is blocked. Therefore, Dma1's dynamic SPB localization is a critical feature of *S. pombe* cytokinesis and silencing of the mitotic checkpoint.

RESULTS

Dma1's E3 ligase activity impacts its abundance and localization

Consistent with previous literature (Guertin *et al.*, 2002; Johnson and Gould, 2011), we observed that Dma1 tagged at its endogenous locus with mNeonGreen (mNG) (Shaner *et al.*, 2013; Willet *et al.*, 2015) (Figure 1A) concentrates at SPBs during mitosis, where it is required for SIN inhibition (Guertin *et al.*, 2002). We also observed localization at cell tips during interphase and at the division site during mitosis and cytokinesis. Given that wild-type Dma1 did not appear to localize to SPBs during the majority of interphase (Figure 1A), we sought to identify the mechanism(s) that influences Dma1 SPB targeting and SIN inhibition.

Because Dma1 localization changes over the course of the cell cycle, we undertook time-lapse imaging experiments to clarify the timing of Dma1 localization to the SPB and cell division site. Dma1-mNG became enriched at SPBs prior to SPB separation (Figure 1B and Supplemental Figure S1A). Unexpectedly, at the onset of mitosis, Dma1-mNG appeared in nodelike structures, a pattern previously undetected for Dma1 (Guertin *et al.*, 2002), that partially overlapped with cytokinetic precursor nodes marked by Rlc1 (Rincon and Paoletti, 2012), before forming a ring at the division site (Figure 1B and Supplemental Figure S1B). Then Dma1-mNG appeared to transiently leave SPBs during anaphase B, returning to them before telophase and then leaving again after cell division (Figure 1, B and C, and Supplemental Figure S1C). In 24 of 28 (86%) mitotic SPBs, Dma1-mNG signal transiently dimmed or became undetectable, whereas the SPB markers Sid4-mCherry or Sad1-mCherry did not. Dma1 SPB dimming occurred within 2 min of anaphase B onset in 90% of cells exhibiting this phenomenon, and it returned to SPBs in all cases before the end of anaphase B, marked by maximal SPB separation, and then left again at cell division. In a few cases, the Dma1 signal was observed to "flicker" on and off a SPB during anaphase B and to shift in intensity between the two SPBs.

Similarly, Dma1-mNG was observed to leave and then return to the division site although with delayed kinetics (min 18–26) compared with what was observed at SPBs (min 14–16) (Figure 1, B and C, and Supplemental Figure S1, A and B). The role of Dma1 at the division site is not yet understood because no binding partners or substrates at the medial cortex have been identified.

Interestingly, in contrast to wild-type Dma1, we found that the Dma1-I194A mutant, which lacks ubiquitin ligase activity due to a mutation in the RING-finger domain (Johnson and Gould, 2011), was detectable at SPBs throughout the cell cycle when it was tagged with mNG (Figure 1D) or GFP (unpublished data) at its C-terminus, or either fluorophore at its N-terminus (unpublished data). Dma1-I194A-mNG signal persisted at SPBs throughout the cell cycle, only detectably dimming at 14% of mitotic SPBs, although its dynamic localization at the cell division site appeared like wild type (Figure 1E and Supplemental Figure S1). Also, in 20 of 20 cells Dma1-I194A-mNG localized more intensely at one of the two SPBs for most of mitosis (Figure 1, E and F). Thus, Dma1 localization is more dynamic than previously appreciated, and Dma1 catalytic activity affects its SPB dynamics. Because Dma1 activity does not impact its cell division site localization dynamics, a different mechanism of targeting to this site must be in place.

Sid4 ubiquitination does not impact Dma1 accumulation at SPBs

To determine why Dma1-I194A was less dynamic at SPBs during mitosis than Dma1, we examined whether the ubiquitination status of either of Dma1's two known substrates, Sid4 and Dma1 itself (Johnson and Gould, 2011), modulated its localization. To investigate whether the absence of Sid4 ubiquitination promoted Dma1 localization to SPBs, we first needed to develop a strain in which Sid4 ubiquitination was abrogated. The canonical approach is to replace target lysines with arginines; however, previous attempts to construct such a Sid4 variant were unsuccessful (Johnson and Gould, 2011; Johnson *et al.*, 2013). We therefore turned to a method described previously to eliminate ubiquitination of a protein of interest—fusion to a deubiquitinating enzyme (DUB) catalytic domain (Stringer and Piper, 2011).

To identify the appropriate DUB for fusion to Sid4, we screened 18 of the 20 *S. pombe* DUBs for their ability to rescue Dma1 overexpression-induced cytokinesis failure and cell death when the DUB was also overproduced (Murone and Simanis, 1996; Guertin *et al.*, 2002). Four of the 18 DUBs (Ubp1, Ubp2, Ubp7, and Ubp14) suppressed Dma1-induced cell death when they were coordinately overproduced, presumably by reversing Sid4 ubiquitination. Of these, only Ubp7 has diffuse cytoplasmic localization and functions independently of other subunits in vivo (Kouranti *et al.*, 2010), making it well suited for our purpose. The ubiquitin specific protease (USP) domain of Ubp7 was fused to the C-terminus of Sid4 (Sid4-DUB) and produced under control of the native *sid4*$^{+}$ promoter as the sole version of Sid4 in the cell. The fusion did not affect cell viability, but the Sid4-DUB fusion was still ubiquitinated (Supplemental Figure S2A), indicating that the DUB was not able to access Sid4 ubiquitination sites.

We next tested whether adding the Ubp7 USP domain to the C-terminus of the Sid4 binding partner Ppc89 (Rosenberg *et al.*, 2006) eliminated Sid4 ubiquitination. The Ppc89-Ubp7 USP fusion (hereafter called Ppc89-DUB) abolished Sid4 ubiquitination, comparable to deletion of *dma1* (Supplemental Figure S2B). The *ppc89-DUB* strain grew similarly to wild type at a variety of temperatures (Supplemental Figure S2C), and as would be expected when Sid4 cannot accumulate ubiquitin modifications, the *ppc89-DUB* strain resisted Dma1 overexpression-induced cell death (Supplemental Figure S2D).

To determine whether lack of Sid4 ubiquitination affected Dma1-mNG localization, we measured and compared Dma1-mNG SPB intensity relative to Sad1-mCherry in *wild-type* and *ppc89-DUB* strains and found no difference (Supplemental Figure S2, E and F). Moreover, the dynamic localization of Dma1-mNG to the SPB and division site was unchanged in the *ppc89-DUB* strain, although mitotic progression took longer in this strain; of 22 SPBs examined in 11 cells,

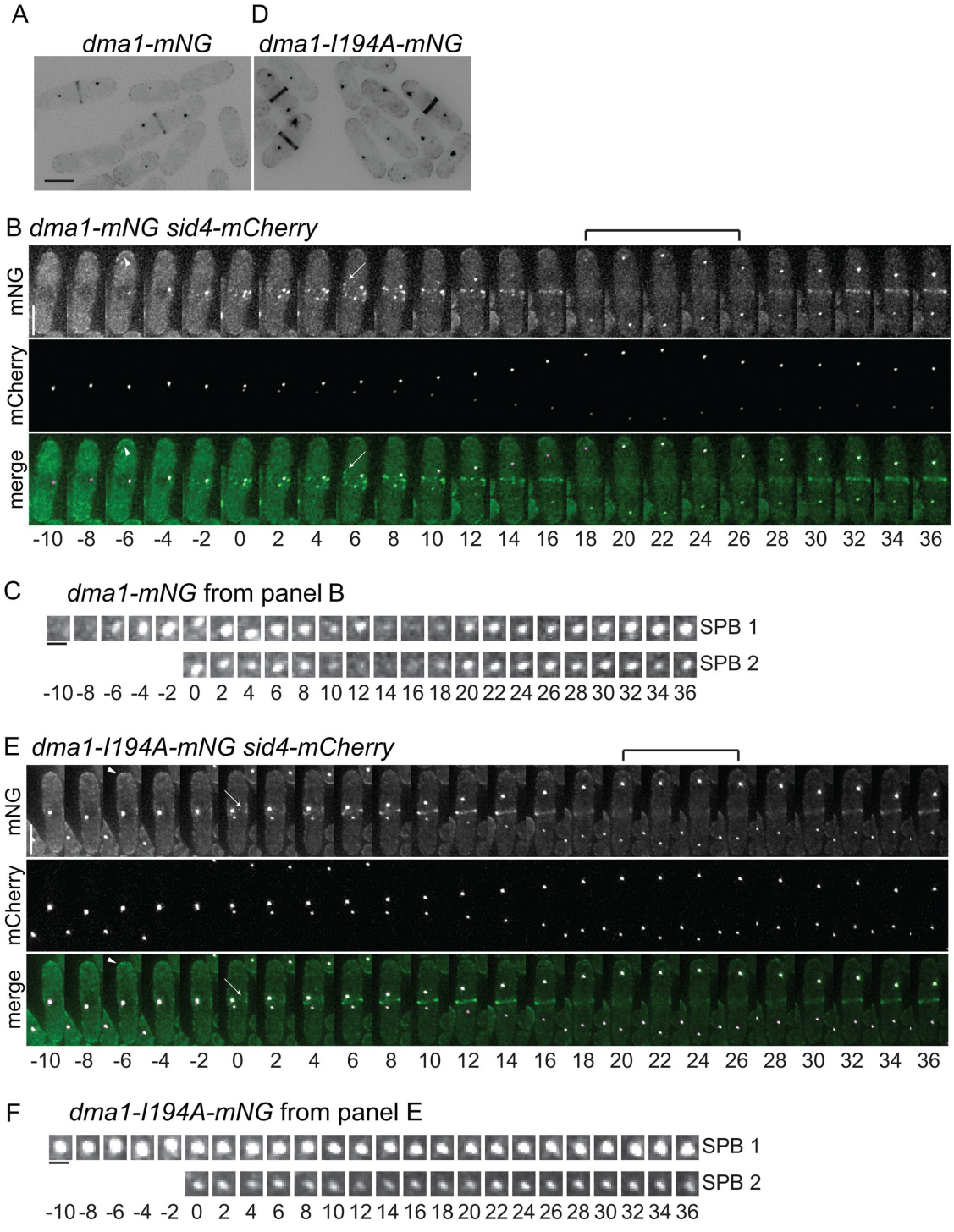

FIGURE 1: Dynamics of Dma1 localization through the cell cycle. (A, D) Live cell images of *dma1-mNG* (A) and *dma1-I194A-mNG* (D). Scale bar, 5 μm. (B, E) Images from representative movies of *dma1-mNG sid4-mCherry* (B) and *dma1-I194A-mNG sid4-mCherry* (E). Arrows indicate Dma1 localization in cytokinetic nodelike structures. Arrowheads indicate Dma1 localization to cell tips. Brackets indicate times of reduced Dma1 detection at the division site. Time in minutes denoted below images; 0 indicates initial frame of SPB separation. Scale bars, 5 μm. (C, F) Enlarged SPB region(s) from movies in B and E. Scale bars, 1 μm.

Dma1-mNG was transiently undetectable on 17 and diminished on 5 others during anaphase (Supplemental Figure S2, G and H). These data demonstrate that an absence of Sid4 ubiquitination does not account for the differences observed in catalytically inactive Dma1 dynamic localization at SPBs relative to wild-type Dma1.

Dma1 exhibits promiscuous autoubiquitination in vivo and in vitro

In addition to displaying distinct dynamics, by comparing Dma1-mNG and Dma1-I194A-mNG intensities normalized to the SPB marker Sad1-mCherry (Hagan and Yanagida, 1995), we found that

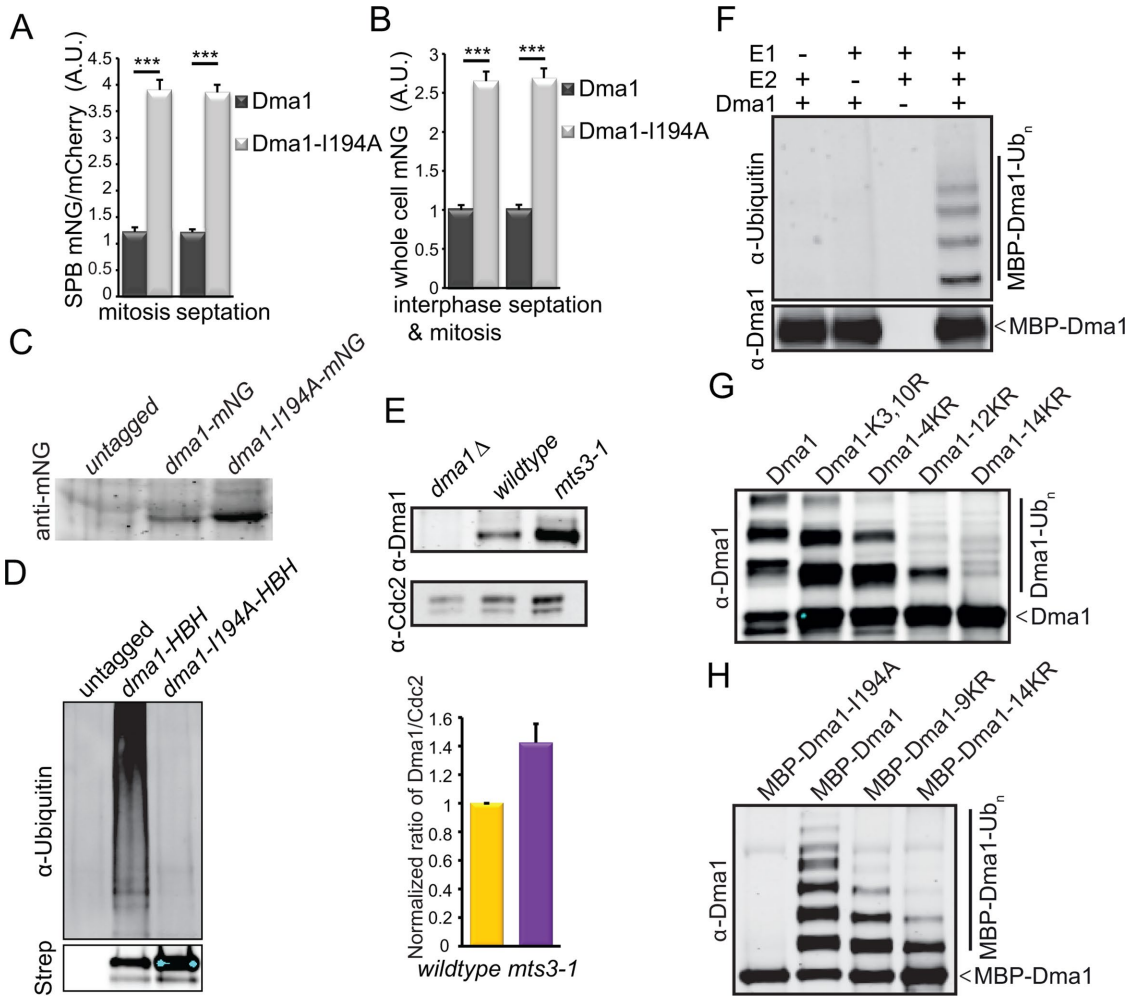

FIGURE 2: Dma1 autoubiquitination influences its abundance and localization dynamics. (A) Quantification of Dma1-mNG and Dma1-I194A-mNG intensities at SPBs, relative to Sad1-mCherry in mitotic or septated cells. $n \geq 42$ cells for each measurement; error bars represent standard error determined by two-tailed Student's *t* test, $^{***}p = 4.9 \times 10^{-43}$ (mitosis) and 1.3×10^{-11} (septation). A.U. = arbitrary units. (B) Quantification of Dma1-mNG and Dma1-I194A-mNG whole-cell fluorescence intensities in nonseptated interphase and mitotic cells or septated cells; $n \geq 20$ cells for each measurement. Error bars represent standard error determined by two-tailed Student's *t* test, $^{***}p = 1.3 \times 10^{-7}$ (interphase and mitosis) and 4.9×10^{-9} (septation). A.U. = arbitrary units. (C) Abundance of Dma1-I194A-mNG relative to wild-type Dma1-mNG was determined by immunoblotting. One representative blot of three independent repetitions is shown. (D) Dma1-HBH, Dma1-I194A-HBH, or nonspecifically purified proteins were isolated from *mts3-1* cells that had been shifted to 36°C for 3 h. Dma1 ubiquitination was detected by immunoblotting with an antiubiquitin antibody (top panel) and unmodified Dma1 was detected with fluorescently labeled streptavidin (bottom panel). (E) Relative protein levels of Dma1 (top) in the indicated strains as determined by immunoblotting immunoprecipitates relative to Cdc2 in the lysates (bottom) (top panel) followed by quantification with Odyssey (bottom panel). Quantification data is average ± SD from two independent experiments. (F) Recombinant MBP-Dma1 was incubated with an E1-activating enzyme and/or the E2-conjugating enzyme, UbcH5a/UBE2D1, and methylated ubiquitin. Ubiquitin-modified Dma1 was detected by immunoblotting with an anti-ubiquitin antibody (top panel) and unmodified Dma1 was detected with anti-Dma1 serum (bottom panel). (G) Recombinant MBP-Dma1 proteins were incubated with an E1-activating enzyme, the E2-conjugating enzyme UbcH5a/UBE2D1 and methylated ubiquitin. Dma1 was cleaved from MBP and autoubiquitination was detected by immunoblotting with anti-Dma1 serum. (H) Recombinant MBP-Dma1 proteins were incubated with an E1-activating enzyme, the E2-conjugating enzyme UbcH5a/UBE2D1, and methylated ubiquitin. MBP-Dma1 ubiquitination was detected by immunoblotting with anti-Dma1 serum.

Dma1-I194A-mNG was more abundant (3.2-fold) at SPBs in both mitotic and septated cells compared with wild-type Dma1 (Figure 2A). Although we did not quantitate Dma1-I194A abundance at the division site or cell tips, it was visibly more intense than wild-type Dma1 at these sites as well (Figure 1D).

To determine whether the different intensities measured at SPBs reflected increased abundance of Dma1-I194A relative to wild-type Dma1, we examined protein levels by whole cell fluorescence intensity and immunoblotting (Figure 2, B and C). By both methods, the mutant protein was 2.6-fold higher in abundance, indicating that inactivating the catalytic activity of Dma1 causes an increase in total Dma1 protein. However, the overall difference in protein abundance was not as high as the difference in SPB intensity (2.6-fold increase vs. 3.2-fold increase) and so cannot fully

account for the increased protein and lack of dynamics of Dma1-I194A observed at SPBs. Dma1 autoubiquitinates in vitro (Johnson *et al.*, 2012a; Wang *et al.*, 2012). Therefore, we next asked whether a lack of autoubiquitination in catalytically inactive Dma1-I194A could explain its increased SPB localization and decreased SPB localization dynamics.

To establish that Dma1 autoubiquitinates in vivo, Dma1 and Dma1-I194A, both tagged with his_6-biotin-his_6 (HBH), were purified under fully denaturing conditions and probed for the presence of ubiquitinated forms by immunoblotting. Using the *mts3-1* proteasome mutant to block turnover of ubiquitinated proteins, we detected ubiquitin modification of wild-type Dma1 but not catalytically inactive Dma1-I194A (Figure 2D) (Gordon *et al.*, 1996). Thus, Dma1 autoubiquitinates in vivo as well as in vitro.

To test the idea that Dma1 autoubiquitination might promote its proteasomal degradation, we measured Dma1 levels in *mts3-1* relative to wild type and found that Dma1 was more abundant in *mts3-1*-arrested cells (Figure 2E). These data are consistent with autoubiquitination triggering Dma1 destruction.

To investigate directly whether ubiquitin modifications affect Dma1's ability to localize to SPBs, we sought to identify and mutate the autoubiquitinated residues. We first examined the sites of Dma1 autoubiquitination in vitro using recombinant Dma1 (Figure 2F) (Johnson *et al.*, 2012a; Wang *et al.*, 2012). Dma1 contains 14 lysines that could be targeted for autoubiquitination. A series of mutants containing increasing numbers of lysine to arginine mutations was generated recombinantly and assayed for autoubiquitination using methyl ubiquitin to prevent chain elongation. Though the number of ubiquitin moieties added to Dma1 decreased with decreasing availability of lysines, only lysine-less Dma1 (Dma1-14KR) was completely unmodified (Figure 2G). Dma1 also ubiquitinated its maltose-binding protein (MBP) tag if the tag was not removed prior to the ubiquitination reaction (Figure 2H), indicating that Dma1 promiscuously ubiquitinates lysines in its proximity.

To determine which Dma1 lysines are ubiquitinated in vivo, we performed LC-MS/MS analyses on Dma1 purified from cells at different cell-cycle stages. Nine ubiquitinated lysines of the 14 possible were identified (Supplemental Figures S3A-I and S4A). We constructed mutant strains in which the 9 identified modified lysines or all 14 lysines in the protein were substituted with arginine (9KR and 14KR, respectively). Surprisingly, both Dma1 mutants tagged endogenously with the HBH tag were ubiquitinated (Supplemental Figure S4B). The abundance of Dma1-14KR was significantly reduced, likely because so many mutations disrupted its structure (Supplemental Figure S4B). However, that both were still ubiquitinated, combined with the ability of Dma1 and Dma1-14KR to ubiquitinate an MBP tag in vitro (Figure 2H), suggested that tags on the protein could be ubiquitinated in lieu of, or in addition to, Dma1 lysines. Indeed, LC-MS/MS analyses of Dma1-TAP and Dma1-HBH purified from cells identified ubiquitinated lysine residues in both tags (Supplemental Figure S3, J and K), confirming that Dma1 ubiquitinates its tags both in vitro and in vivo. Therefore, we predict that although the Dma1-9KR-mNG and Dma1-14KR mutants exhibited wild-type localization dynamics (Supplemental Figure S4, C and D; unpublished data), this is because Dma1 is still able to ubiquitinate the mNG tag.

We next reasoned that wild-type Dma1 would be able to autoubiquitinate an inactive form of itself in close proximity and therefore restore wild-type dynamics to the catalytically inactive mutant. To test this, we constructed three diploid strains containing one mNG-tagged allele: *dma1-mNG/dma1*$^+$; *dma1-I194A-mNG/dma1*$^+$; *dma1-I194A-mNG/dma1-I194A*. When both alleles were wild type or both inactive, the localization dynamics of the tagged protein mirrored the haploid situation, with Dma1-mNG dimming or disappearing from 100% of 20 SPBs during anaphase (Figure 3, A and D) and Dma1-I194A-mNG showing no change at 84% of 44 SPBs (Figure 3, B and E). In contrast, when Dma1-I194A-mNG was combined with wild-type Dma1, the tagged inactive protein now exhibited dynamics similar to wild type, with the Dma1-I194A-mNG signal dimming or disappearing at 93% of 28 SPBs during anaphase (Figure 3, C and F). This result indicates that the untagged wild-type Dma1 ubiquitinates the inactive Dma1-I194A-mNG, a reaction that could occur in *cis* or *trans* because Dma1 is a dimer (Johnson *et al.*, 2012a). These results are consistent with a model in which autoubiquitination triggers the transient loss of Dma1 from SPBs during early anaphase B to allow SIN activation.

To test directly whether Dma1 autoubiquitination prevents its binding to phosphorylated Sid4, a step necessary for SIN inhibition, full-length Dma1 was purified from bacteria. Like the FHA domain alone (Johnson *et al.*, 2013), full-length Dma1 preferentially bound phosphorylated Sid4 peptide (Figure 4A). When Dma1 was allowed to autoubiquitinate prior to the binding reaction, it did not bind the Sid4 phosphopeptide, and the ubiquitinated Dma1 was detected in the supernatant (Figure 4, A and B). To clearly detect unbound ubiquitinated Dma1, the supernatants of the binding reaction were incubated with USP2, a commercially available deubiquitinating enzyme that shows activity towards multiple types of ubiquitin chains in vitro (Komander *et al.*, 2009). USP2 treatment allowed detection of Dma1 in the supernatants and confirmed that it did not bind the beads (Figure 4A), confirming that Dma1 can interact with Sid4 phosphopeptide only if it is not ubiquitinated. If Dma1 was bound to the Sid4 phosphopeptide before the ubiquitination reaction, then it was released into the supernatant upon ubiquitination (Figure 4, C and D). These data support the idea that autoubiquitination at the onset of anaphase B triggers Dma1 removal from phosphorylated Sid4 at SPBs to allow SIN activation.

Relationship between Dma1 SPB dynamics and the SIN

The dynamic localization of Dma1 during mitosis is reminiscent of that displayed by several SIN components (Johnson *et al.*, 2012b; Simanis, 2015). Asymmetric SPB localization of Cdc7 to one SPB and localization of Sid2 to the division site are considered markers of maximal SIN activation and Cdk1 inhibition (Johnson *et al.*, 2012b; Simanis, 2015). Therefore, we imaged Dma1-mNG in combination with those two SIN components (Figure 5) to place the timing of dynamic Dma1 localization in the context of SIN activation. Dma1-mNG SPB dimming occurred 1–2 min in 14 cells and 3–5 min in three cells prior to the development of detectable asymmetry in Cdc7-mCherry signal in the 17 cells examined (Figure 5, A and B), and the transient reduction in Dma1 division site localization preceded Sid2 division site localization in all 8 cells examined (Figure 5C).

To test whether SIN activity modulated Dma1's localization pattern, Dma1-mNG was imaged in the SIN mutant *cdc7-24* as cells passed through mitosis. Dma1-mNG intensity dimmed or disappeared at 21 of 22 SPBs in 11 cells, but it never reintensified at SPBs as in wild-type cells (Figure 6, A and B), indicating that SIN activity is important for Dma1 reaccumulation at SPBs in late anaphase. Dma1 did reintensify at the division site in all 11 cells examined. We next imaged Dma1-mNG in the hyperactive SIN mutant *cdc16-116*. In these cells that have constitutive SIN activity (Fankhauser *et al.*, 1993), Dma1-mNG was detected on 97% (116/119) of SPBs (Figure 6C). Since in wild-type cells the SIN is not maximally active until Cdk1 activity falls later in anaphase (He *et al.*, 1997; Guertin *et al.*, 2000; Dischinger *et al.*, 2008), these results raise the possibility that

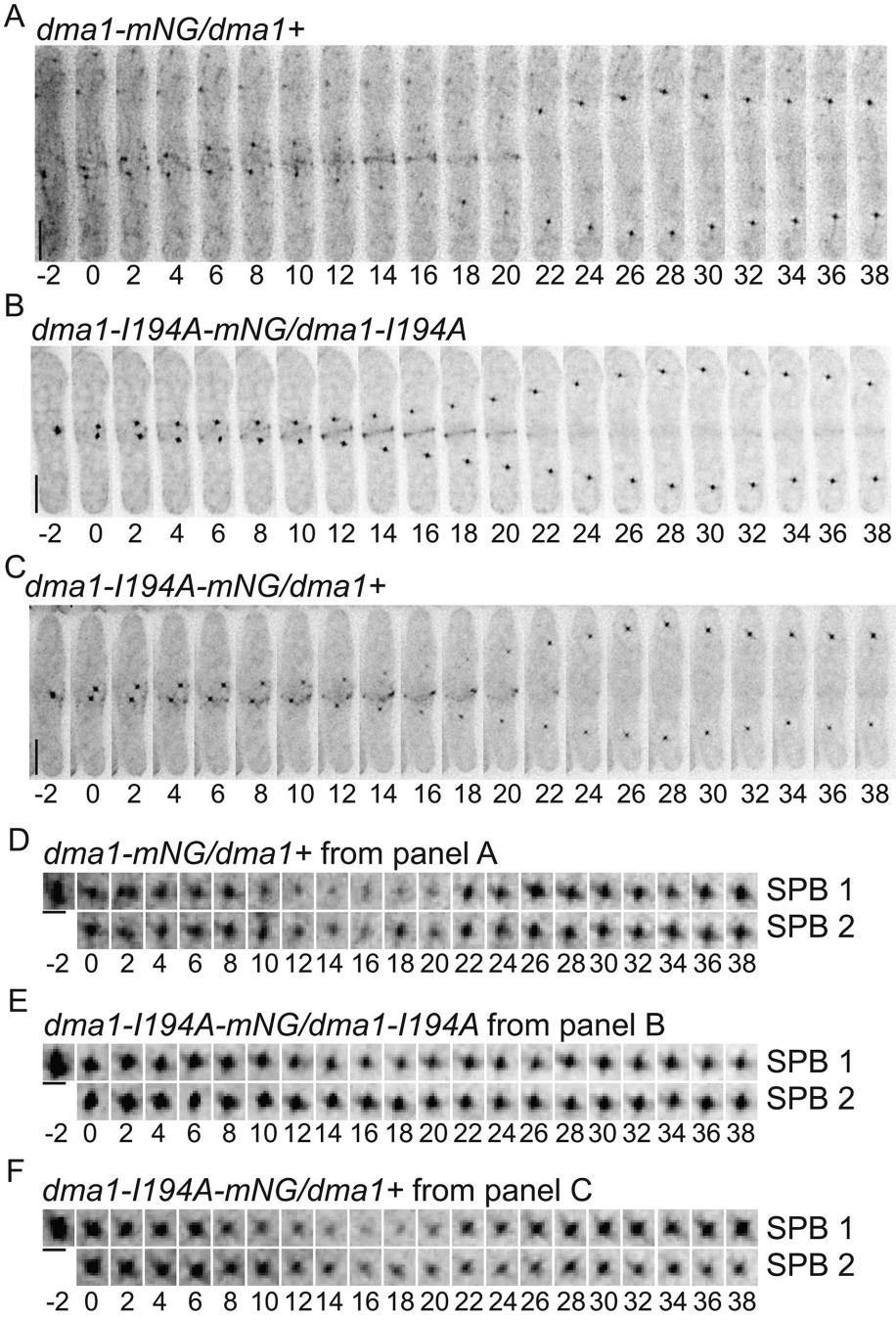

FIGURE 3: Dma1 catalytic activity drives its localization dynamics. (A–C) Images from representative movies of *dma1-mNG/dma1+* (A), *dma1-I194A-mNG/dma1-I194A* (B), and *dma1-I194A-mNG/dma1+* (C). Time in minutes denoted below images. Time 0 indicates initial frame of SPB separation. Scale bars, 5 µm. (D–F) Enlarged SPB region(s) from movies in A–C. Scale bars, 1 µm.

high SIN activity promotes Dma1 SPB reaccumulation at the end of anaphase.

Constitutive Dma1 localization to SPBs prevents cytokinesis

We next wanted to determine the importance of Dma1 transiently cycling off of SPBs during anaphase B by permanently tethering it to SPBs. To do this, we tagged Sid4 at its endogenous locus with GFP-binding protein (GBP), which has a high affinity for GFP (Rothbauer *et al.*, 2006, 2008). When a *sid4-GBP-mCherry* or *sid4-GBP* strain was crossed to *dma1-GFP*, many double mutants (31/35 and 7/19, respectively) were dead. Similarly, synthetic lethality was previously observed when the tags were reversed and *dma1-GBP-mCherry* was expressed in a *sid4-GFP* strain (Chen *et al.*, 2017), although in this study, colocalization at SPBs and dependency of cell death on failed cytokinesis was not determined. Fortunately, we were able to recover some double-tagged strains for imaging, although they grew very poorly: 22% of *dma1-GFP sid4-GBP-mCherry* and 11% of *dma1-GFP sid4-GBP* cells were dead or lysing. In live *dma1-GFP sid4-GBP-mCherry* cells, Dma1-GFP localized to the division site normally and colocalized with Sid4-GBP-mCherry at SPBs at all stages of the cell cycle (Figure 7A), indicating that Dma1-GFP was tethered permanently to SPBs. In both double mutant strains, there was a higher percentage of multi-nucleated cells than in wild type and 46% of binucleated cells had "kissing" nuclei (Figure 7, B–D), indicative of SIN failure (Hagan and Hyams, 1988). We reasoned that if the SIN was inhibited in these strains via Dma1-mediated Sid4 ubiquitination, introducing the *ppc89-DUB* fusion allele that prevents Sid4 ubiquitination (Supplemental Figure S2B) should rescue growth of *dma1-GFP sid4-GBP-mCherry* cells. As predicted, of the 14 *dma1-GFP sid4-GBP-mCherry ppc89-DUB* triple mutant strains constructed, all were viable and showed reduced levels of multinucleation and "kissing" nuclei (Figure 4D). These data indicate that constitutive association of Dma1 with Sid4 drives Sid4 ubiquitination, compromises SIN activity, and results in cytokinesis failure. Thus, Dma1's transient loss from SPBs at the onset of anaphase must be a critical step in silencing the mitotic checkpoint, as well as allowing cytokinesis to proceed in unperturbed cells.

DISCUSSION

SPB localization of the ubiquitin ligase Dma1 is required for its function in a mitotic checkpoint that stalls cytokinesis through SIN inhibition when a mitotic spindle cannot form (Murone and Simanis, 1996; Guertin *et al.*, 2002). In this report, we show that Dma1 exhibits previously unrecognized dynamic localization to SPBs and the cell division site during anaphase. We found that both the SIN and autoubiquitination modulate Dma1 SPB localization dynamics, and therefore its function, in the checkpoint. Further, our data show that if Dma1 is prevented from leaving Sid4 on the SPBs, cells fail division, indicating that Dma1's transient loss from SPBs is a critical step in cytokinesis and cell survival.

Dma1 division site localization

Though Dma1 was previously shown to localize to the division site (Guertin *et al.*, 2002), our time-lapse imaging experiments with the

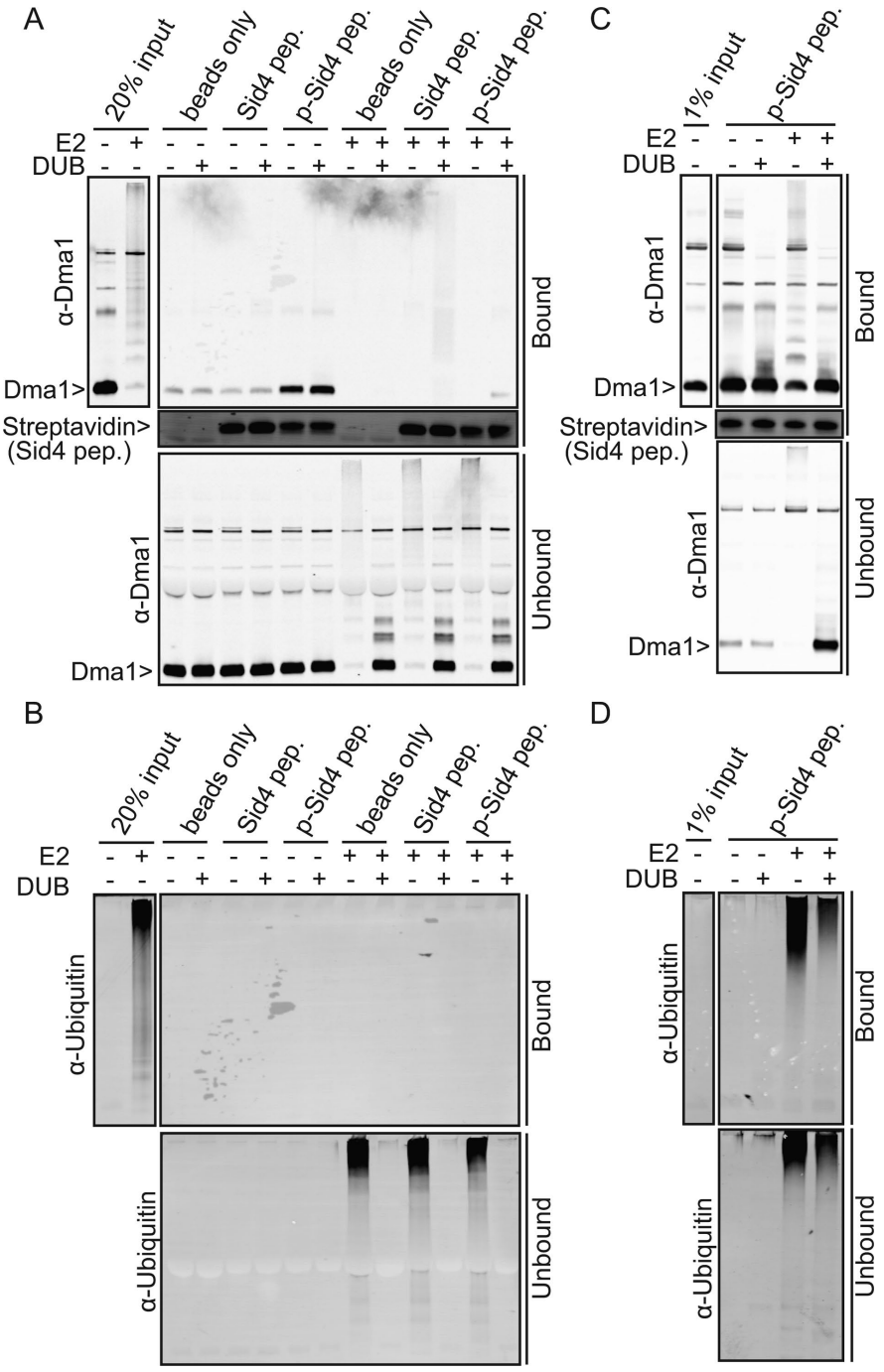

FIGURE 4: Dma1 ubiquitination disrupts its interaction with Sid4. (A) Recombinant Dma1 was incubated with E1, Ub, and E2 (+E2) or not (–E2), followed by incubation with biotinylated Sid4 peptides (either unphosphorylated [Sid4] or phosphorylated [p-Sid4]) conjugated to streptavidin beads. Beads only was included as a control. Supernatants (containing unbound Dma1) and beads (containing bound Dma1) were recovered, and each was split in half for treatment either with H_2O, or USP2 to collapse ubiquitinated Dma1 for better detection. The entire samples from beads (top panel) and half of the supernatants (lower panel) were resolved by SDS–PAGE and detected by immunoblotting with anti-Dma1 serum or streptavidin (for visualization of biotinylated peptides). (B) Anti-Ub blotting of the same membranes blotted for anti-Dma1 in A. (C) Recombinant Dma1 was incubated with biotinylated phosphorylated Sid4 (p-Sid4) peptides. The beads were split in half and subjected to in vitro ubiquitination assay with (+E2) or without (–E2) E2 enzyme. Supernatants (containing unbound Dma1) and beads (containing bound Dma1) were recovered and each was split in half for treatment with either H_2O or USP2. The entire samples from beads (top panel) and supernatants (bottom panel) were resolved by SDS–PAGE and detected by immunoblotting with anti-Dma1 serum or streptavidin. (D) anti-Ub blotting of the same membranes blotted for anti-Dma1 in C.

brighter mNG fluorophore (Shaner *et al.*, 2013) revealed more detail. Dma1-mNG initially appears in nodelike structures, reminiscent of cytokinetic precursor nodes (Rincon and Paoletti, 2012), before coalescing into a ring. In addition, Dma1 leaves the division site after anaphase B onset and before ring constriction and then reappears at the division site before cell division. The role of Dma1 at the division site is not yet understood, because no binding partners or substrates at the medial cortex have been identified. Because neither Dma1 activity nor the SIN impacts its cell division site localization dynamics, a different mechanism of targeting to this site must be in place. Importantly, tethering Dma1 to Sid4 at the SPB using the GBP-GFP system blocked cytokinesis without disrupting Dma1 localization to the division site, validating that it is Dma1's SPB localization that is important for controlling SIN function. We also detected Dma1 localization to cell tips in this study, but, again, its mechanism of targeting and function there are not known.

SIN regulation of Dma1 dynamics

Although the transient dip in Dma1 SPB localization in early anaphase depends on its catalytic activity and is independent of SIN function, SIN activity is required for Dma1's reaccumulation at SPBs later in anaphase. This observation may reflect a change in Dma1's autoubiquitination activity or that of a counteracting deubiquitinating enzyme or reveals a component of negative feedback in which the SIN activates an inhibitor to direct its own silencing (Garcia-Cortes and McCollum, 2009). Since Dma1 is a phosphoprotein (Koch *et al.*, 2011), it will be interesting to determine the role of phosphorylation in Dma1 regulation and whether this is controlled directly or indirectly by SIN kinases.

Dma1 autoubiquitination controls its dynamic localization at SPBs

Our data show that Dma1 is capable of extensive autoubiquitination in vitro and in vivo. Its promiscuous autoubiquitination, which extended to any tag that we tested that includes lysines, complicated our investigation of its role as we were unable to visualize the dynamic localization of a lysine-less, catalytically active Dma1 protein with confidence in a haploid cell. However, we were able to use heterozygous diploids to show that the active form of the protein was sufficient to remove the inactive form from SPBs during early anaphase. Indeed, our data support the idea

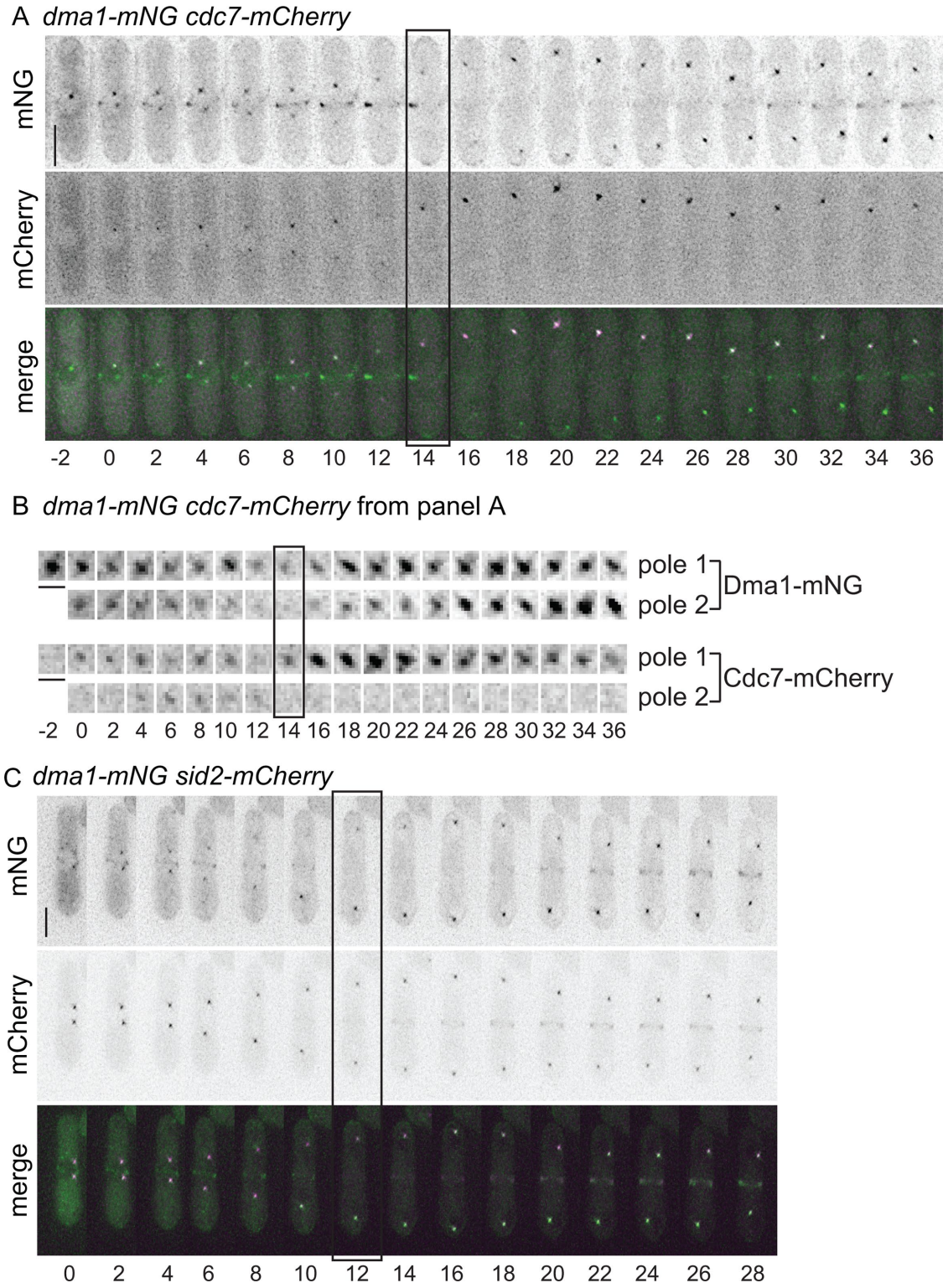

FIGURE 5: SPB dynamics of Dma1 relative to SIN components. Images from representative movies of *dma1-mNG cdc7-mCherry* (A) and *dma1-mNG sid2-mCherry* (C). Time in minutes denoted below images. In A, time 0 indicates initial frame of SPB separation while in C, time 0 indicates the beginning of imaging. Scale bars, 5 μm. (B) Enlarged SPB region(s) from movie in A. Scale bars, 1 μm. In A and B, boxes indicate initial frame of asymmetric Cdc7 SPB localization. In C, the box indicates the first frame Sid2 localization to the division site was detected.

that autoubiquitination at the onset of anaphase triggers transient Dma1 removal from SPBs to allow full SIN activation (Figure 7E). Preventing Dma1 from leaving the SPB using the GBP trap inhibited the SIN. These results are consistent with the role of Dma1 as a SPB-localized SIN antagonist in early mitosis whose function must be relieved at the onset of anaphase (Guertin *et al.*, 2002; Johnson and Gould, 2011; Johnson *et al.*, 2013).

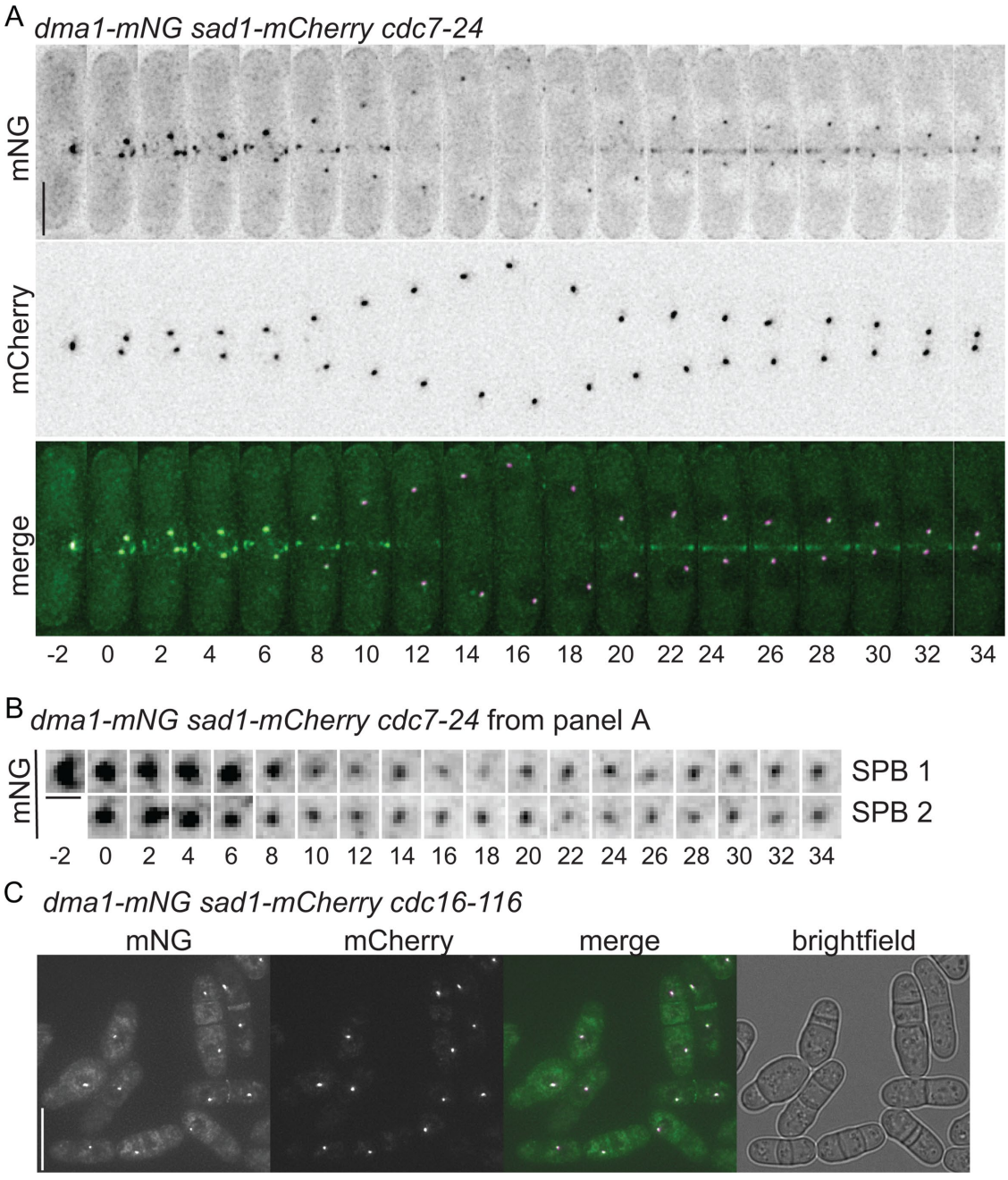

FIGURE 6: Influence of SIN function on Dma1 localization dynamics. (A) Images from a representative movie of *dma1-mNG sad1-mCherry cdc7-24* following shift to 36°C for 2 h. Time in minutes denoted below images; time 0 indicates initial frame of SPB separation. Scale bar, 5 μm. (B) Enlarged SPB region(s) from movie in A. Scale bars, 1 μm. (C) Representative live cell image of *dma1-mNG sad1-mCherry cdc16-116* shifted to 36°C for 3 h. Scale bar, 10 μm.

Degradation of Dma1

Because the catalytically inactive form of Dma1 is more abundant than wild type, its levels are clearly regulated by its own activity state. While we do not yet know all the factors modulating Dma1 catalytic activity, our data are consistent with autoubiquitination triggering Dma1 destruction. This could happen directly at SPBs, analogously to proteasome-mediated degradation of many regulatory proteins at centrosomes (Vora and Phillips, 2016), or off the centrosome if ubiquitination prevents Dma1 association with its SPB tethers, similarly to what has been observed for another SIN inhibitor, Byr4 (Krapp *et al.*, 2008). This mechanism of inhibiting Dma1, autoubiquitination and self-destruction, may be broadly applicable in signaling pathways when the outcome of substrate ubiquitination is not degradation and signal flux through a pathway must be restored rapidly. Dma1 relatives CHFR and RNF8 are integral components of checkpoint pathways that undergo autoubiquitination in vivo and in vitro (Kang *et al.*, 2002; Lok *et al.*, 2012), but whether this modification is a key step in checkpoint silencing in their cases remains to be determined. To fully understand the factors that modulate the Dma1-dependent mitotic checkpoint, it will be important to determine how Dma1 autoubiquitination is restrained to allow substrate ubiquitination during

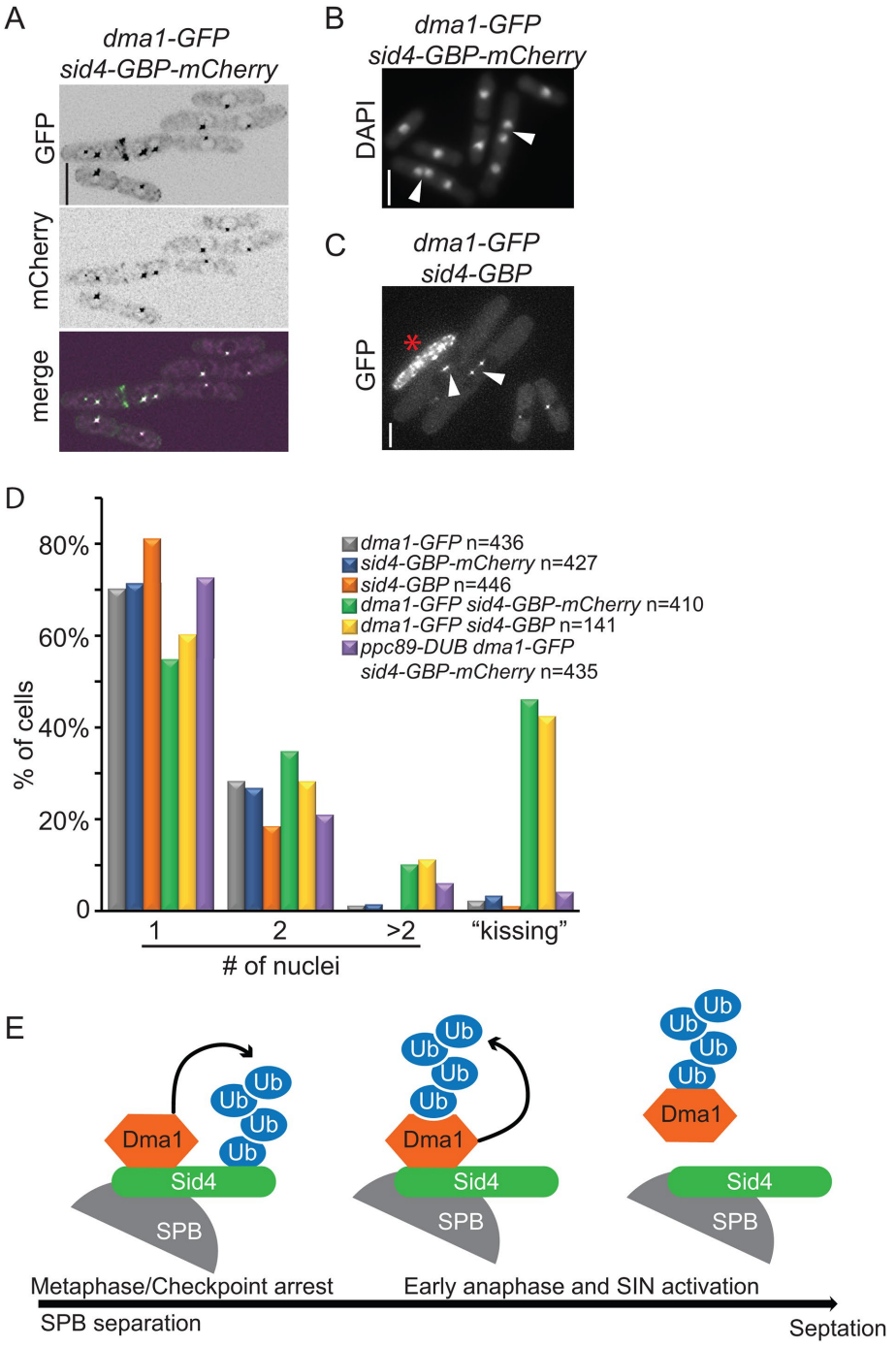

FIGURE 7: Dma1 must leave the SPBs for cytokinesis. (A) Representative live cell images of *dma1-GFP sid4-GBP-mCherry*. (B) Representative DAPI stained images of *dma1-GFP sid4-GBP-mCherry*. (C) Representative image of *dma1-GFP sid4-GBP* cells illustrating "kissing nuclei" phenotype indicated with arrows in B and C. Scale bars in A and B, 10 µm; in C, 5 µm. (D) Quantification of cells from B and C with 1, 2, and >2 nuclei and separately "kissing nuclei." (E) Cartoon showing the dynamic localization of Dma1 throughout mitosis and cytokinesis. In metaphase when the mitotic checkpoint is activated, Dma1 binds and ubiquitinates Sid4. Our data indicate that in early anaphase, Dma1 autoubiquitinates and leaves the SPB allowing maximal SIN activation and cytokinesis.

early mitosis. It will also be important to understand the checkpoint silencing strategies used in other organisms to allow cytokinesis to proceed following chromosome clearance from the division site and whether there are parallels with the strategies used by fission yeast.

MATERIALS AND METHODS

Yeast

Yeast strains grown in this study (Supplemental Table S1) were grown in yeast extract (YE), 4X concentrated yeast extract (4X YE), or minimal media supplemented with leucine and uracil for diploid strains (Moreno *et al.*, 1991). Genes were tagged at the 3′ end of their open reading frame with *mNG:kan*R, *mNG:Hyg*R, *GFP:kan*R, *mCherry:kan*R, *mCherry:nat*R, *HBH:kan*R, HA_3*-TAP:kan*R, *GBP-mCherry:kan*R, or *ubp7*$^+$ (residues 201–875) *DUB:kan*R using PCR and pFA6 cassettes (Wach *et al.*, 1994; Bahler *et al.*, 1998). For gene replacements, a haploid *dma1::ura4*$^+$ strain was transformed with the appropriate pIRT2–*dma1* mutant, and integrants were selected by resistance to 1.5 mg/ml 5-fluoroorotic acid and validated by colony PCR and DNA sequencing. Diploid strains were made by crossing *ade6-M210* cells with *ade6-M216* cells on glutamate plates for 24–48 h followed by restreaking to single colonies on MAU plate and incubating at 32°C for 3 d. White colonies (diploid cells) were then picked for subsequent analysis. For spot assays, cells were cultured in YE at 29°C. Serial 10-fold dilutions of each culture were made, 3 µl of each dilution was spotted on YE plates, and they were incubated at various temperatures for 3–4 d. *nda3-KM311* cultures were grown at 32°C and then shifted to 18°C for 6 h to block in prometaphase. *mts3-1* cells were grown at 25°C and then shifted to 36°C for 3.5 h before imaging or biochemical experiments.

Molecular biology

Plasmids were generated by standard molecular biology techniques. *dma1* mutations were made either in the context of a gene fragment in the pIRT2 vector that included 500 base pairs upstream and downstream of the open reading frame or in the context of the open reading frame in pMAL-c2 vector using a QuikChange site-directed mutagenesis kit (Agilent Technologies). The K to R mutation abbreviations are as follows: Dma1-4KR = K3R, K10R, K121R, and K124R; Dma1-9KR = K3R, K26R, K54R, K82R, K124R, K164R, K174R, K237R, and K262R; Dma1-12KR = Dma1-4KR mutations plus K22R, K26R, K162R, K164R, K174R, K217R, K237R, and K262R; Dma1-14KR = Dma1-12KR mutations plus K54R, and K82R.

cDNAs encoding Ubp2, Ubp3, Ubp4, Ubp8, Ubp14, Ubp15, Ubp16, and Uch1 were amplified by PCR from genomic *S. pombe* DNA using primers containing restriction sites. PCR products were digested with restriction enzymes (*Nde*I/*Bam*HI for *ubp2* and *ubp3* and *Nde*I/*Xma*I for *ubp4*, *ubp8*, *ubp14*, *ubp15*, *ubp16*, and *uch1*),

subcloned into pREP1, and verified by sequencing. DNAs encoding Ubp1, Ubp7, Ubp9, Ubp11, Otu1, Otu2, and Sst2 were digested from genomic constructs, subcloned into pREP1, and verified by sequencing. *ubp6* and *uch2* cDNAs in pREP1 vectors were gifts from Colin Gordon (Stone *et al.*, 2004).

Microscopy

Unless otherwise indicated, all imaging was done at room temperature on a Personal DeltaVision microscope system (Applied Precision) that includes an Olympus IX71 microscope, 60 × NA 1.42 PlanApo oil immersion objective, standard and live-cell filter wheels, a Photometrics CoolSnap HQ2 camera, and softWoRx imaging software. For imaging at 36°C, an environmental chamber with temperature control was used. Time-lapse imaging was done using a CellAsic microfluidic system (EMD Millipore) with appropriate cell media. Figure images are maximum intensity projections of z sections spaced 0.2–0.5 µm apart. Images used for quantification were not deconvolved and sum projected.

Intensity measurements were made with ImageJ software (National Institutes of Health, Bethesda, MD: http://rsbweb.nih.gov/ij/). For all intensity measurements, the background was subtracted by calculating a value for background per pixel (BPP) in the same image as the region of interest (ROI) where there were no cells. The BPP was then multiplied by the area of the ROI, and the resulting product was subtracted from the raw integrated intensity of that ROI yielding the corrected intensity value (Waters, 2009).

For analysis relative to a SPB marker, an ROI was made based on the SPB marker. mNG or GFP fluorescence intensity and mCherry marker fluorescence intensity were measured with background correction for each. Final values for each cell are expressed as mNG/mCherry or GFP/mCherry ratios. Measurements for the cells in each group were averaged for statistical analysis.

Protein purification and mass spectrometry

Endogenously tagged versions of Dma1 (Dma1-HA_3-TAP and Dma1-HBH) were purified as previously described (Gould *et al.*, 2004; Tagwerker *et al.*, 2006; Elmore *et al.*, 2014) and analyzed by 2D-LC-MS/MS as previously described (McDonald *et al.*, 2002; Roberts-Galbraith *et al.*, 2009). RAW files were processed using two pipelines: 1) using Myrimatch (v 2.1.132) (Tabb *et al.*, 2007) and IDPicker (v 2.6.271.0) (Ma *et al.*, 2009) as previously described (McLean *et al.*, 2011) and 2) using turboSEQUEST, Scaffold (v 4.4.7), and Scaffold PTM (v 3.0.0) as previously described (Beckley *et al.*, 2015). We detected the variable di-Gly modification (114 Da) indicating ubiquitination, and these modifications were manually validated (representative spectra are shown in Supplemental Figure S3).

Protein expression and purification

dma1 variants were cloned into pMAL-c2 or pET-His_6-MBP prescission LIC cloning vector (HMPKS) (HMPKS was a gift from Scott Gradia [Addgene plasmid #29721]) for production as MBP fusions. Proteins were induced in *Escherichia coli* Rosetta2(DE3)pLysS cells by addition of 0.8 mM isopropyl-β-D-thiogalactopyranoside (IPTG) and overnight incubation at 18°C. Cells were lysed using 300 µg/ml lysozyme for 20 min followed by sonication. Proteins were affinity purified on prewashed amylose resin (New England Biolabs) in MBP column buffer (100 mM NaCl, 20 mM Tris-HCl, pH 7.4, 1 mM EDTA, 1 mM dithiothreitol [DTT], and 1% Nonidet P-40 [NP-40]). Protein was eluted with 10 mM maltose, and, in some cases, the MBP tag was cleaved with Factor Xa protease (New England Biolabs) or Precission protease (GE Healthcare). Dma1 peak elution fraction(s) were detected by SDS–PAGE and Coomassie Blue (Sigma) staining. After pooling peak fractions, Dma1 proteins were concentrated using a 10 MWCO Amicon Ultra centrifugal filter (EMD Millipore). Dma1 was cleaved from MBP by adding 1 µl (2 units) of PreScission protease to 500 µg MBP-Dma1 on amylose beads (in 200 µl MBP column buffer) and incubating at 4°C overnight. The supernatant containing cleaved Dma1 was retrieved and the concentration of Dma1 was determined by SDS–PAGE using bovine serum albumin (BSA) as standard.

In vitro ubiquitination assay

Ubiquitination reactions included: 0.25–1 µg recombinant MBP-Dma1 (or variant thereof), or Dma1 cleaved from MBP, 175 nM E1 (R&D Systems), 3 µM E2 (R&D Systems), 50 µg/ml methylated ubiquitin, 5 mM ATP, and 1x ubiquitination buffer (50 mM Tris-HCl, pH 7.5, 2.5 mM $MgCl_2$, 0.5 mM DTT). These 20 µl reactions were incubated with agitation at 30°C for 90 min before adding SDS sample buffer or cleaving Dma1 from MBP. For MBP cleavage, 1.8 µl of 1 M $CaCl_2$ and 5 µl Factor Xa were added, and the reactions were incubated at room temperature with agitation for 1 h. Then 100 µl benzamidine beads (1:1 slurry) and 100-µl amylose beads (1:1 slurry) (both prewashed in MBP column buffer) were added, and reactions were incubated at room temperature with agitation for 45 min. Supernatants were transferred to new tubes, and SDS sample buffer was added prior to separation by SDS–PAGE. Ubiquitination products and Dma1 were detected by immunoblotting with anti-ubiquitin (EMD Millipore, MAB1510) at a 1:250 dilution or (Life Sensors, VU-1) at a 1:500 dilution and/or anti-Dma1 (see Supplemental Figure S4E) antibodies.

In vivo ubiquitination assay

Dma1-HBH was purified from 250-ml 4X YE pellets as previously described (Tagwerker *et al.*, 2006; Beckley *et al.*, 2015). Briefly, cell pellets were washed with 10 ml modified buffer 1 (8 M urea, 300 mM NaCl, 50 mM $NaPO_4$, 0.5% Nonidet P-40, and 4 mM imidazole, pH 8, with 1.3 mM benzamidine, 1 mM PMSF, 50 µM PR-619 [LifeSensors], 50 µM *N*-ethylmaleimide, and 1 Complete Protease Inhibitor Cocktail Tablet, EDTA-free [Roche] per 50 ml) and then lysed by bead disruption with 500 µl buffer 1. Lysates were extracted with 10 ml and then 5 ml buffer 1 (15 ml total extraction), cleared by high-speed centrifugation, and then incubated with 200 µl (1:1 slurry) Ni^{2+}-NTA agarose beads (Qiagen) for 3–4 h at room temperature. After incubation, beads were washed four times: one time with 10 ml buffer 1 and three times with 10 ml buffer 3 (8 M urea, 300 mM NaCl, 50 mM $NaPO_4$, 0.5% Nonidet P-40, and 20 mM imidazole, pH 6.3). Proteins were then eluted for 15 min in 5 ml buffer 4 (8 M urea, 200 mM NaCl, 50 mM $NaPO_4$, 0.5% Nonidet P-40 and 2% SDS, 100 mM Tris, and 10 mM EDTA, pH 4.3) two times, and the two eluates were pooled. The pH of the final eluate was adjusted to 8 before 80 µl streptavidin ultra-link resin (Pierce) was added and incubated overnight at room temperature. The streptavidin beads were then washed three times with buffer 6 (8 M urea, 200 mM NaCl, 2% SDS, and 100 mM Tris, pH 8). Purified proteins were detected on a Western blot using an anti-ubiquitin antibody (EMD Millipore, MAB1510) at a 1:250 dilution or (Life Sensors, VU-1) at a 1:500 dilution and fluorescently labeled streptavidin (Li-COR Biosciences).

Biotinylated peptide conjugation to streptavidin beads

A 50% slurry of Ultralink strepavidin beads (20 µl) was washed in 200 µl MBP column buffer three times and resuspended in 88 µl column buffer. The amount of 2 µg (2 µl of 1 mg/ml) synthetic

biotinylated peptides (Genescript) dissolved in 5% acetonitrile was added and incubated at 4°C overnight. Beads were then washed in 200 µl MBP column buffer three times before being resuspended in 10 µl column buffer.

Sid4 phosphopeptide binding assay

The Sid4 phosphopeptide binding assay was performed as described (Johnson *et al*., 2013) with the following modifications. First, 0.5 µg purified recombinant Dma1 (cleaved from MBP-Dma1 by Precission protease) was ubiquitinated in vitro as described above (0.4 µg/µl ubiquitin was used instead of methylated ubiquitin) in the presence (+E2) or absence (–E2) of E2 enzyme in 40 µl total volume for 2 h at 30°C. Reactions were stopped by adding 4 µl 1 M DTT to a final concentration of 91.4 mM. Next, 2.2 µl of the reaction mixture containing 25 ng nonubiquitinated (–E2) or ubiquitinated (+E2) Dma1 was added to 19.8 µl binding buffer (50 mM Tris-HCl, pH 7.4, 25 mM KCl, 5 mM $MgCl_2$, 1 mM DTT) containing streptavidin beads only or 5 µM synthetic biotinylated nonphosphorylated Sid4 peptide (bio-LTSSTCVSSISQ) or phosphorylated Sid4 peptide (bio-LTSSpT_{275}CVpS_{278}SISQ) (Genescript) conjugated on Ultralink streptavidin beads (Pierce) and incubated at 4°C for 30 min (beads were preblocked with 50 µl 5% BSA in binding buffer for 1 h). The unbound supernatants were recovered, split equally into two parts, and treated with 0.33 µl H_2O or 1.5 mg/ml USP2 (Boston Biochem) and analyzed by SDS–PAGE. The beads were washed with 1 ml high-salt MBP column buffer (20 mM Tris-HCl, pH 7.4, 250 mM NaCl, 1 mM EDTA, 0.1% NP-40, 1 mM DTT) five times, followed by washing with 0.5 ml deubiquitination buffer (50 mM Tris, pH 7.4, 25 mM KCl, 5 mM $MgCl_2$, 10 mM DTT) twice prior to being split equally into two parts. Beads were resuspended in 19 µl deubiquitination buffer and treated with 0.33 µl H_2O or USP2. The deubiquitination reactions were incubated with shaking at 32°C for 2 h. Reactions were stopped by adding SDS sample buffer.

Alternatively, phosphorylated Sid4 peptides on beads (6.25 µM) were incubated with 5 ng/µl Dma1 in 200 µl high-salt MBP buffer for 30 min at 4°C in the presence of 5% BSA, followed by 6 × 1 ml wash of high-salt MBP buffer and then with 1 ml of ubiquitination buffer twice. Beads were split into two equal parts (for –E2 and +E2) and subject to the in vitro ubiquitination assay in 20 µl total volume as described above. Reactions were stopped by adding 0.5 µl 1M DTT to a final concentration of 24.9 mM. The unbound supernatants were recovered and split equally into two parts, and 10 µl of 50 mM Tris, 50 mM KCl, 7.5 mM $MgCl_2$ was added (after adjusting the buffer composition is 49.4 mM Tris, 25 mM KCl, 5 mM $MgCl_2$, 12.4 mM DTT) prior to being treated with 0.33 µl H_2O or 1.5 mg/ml USP2. The beads were washed with 1 ml deubiquitination buffer twice and split equally into two parts before treatment with H_2O or USP2 as described above.

Lysis, immunoprecipitation, and immunoblotting

Cell pellets were washed once in NP-40 buffer (10 mM sodium phosphate, pH 7.0, 1% N-P-40, 150 mM NaCl, 2 mM EDTA) with inhibitors (1.3 mM benzamidine, 1 mM PMSF, and 1 Complete Protease Inhibitor Cocktail Tablet, EDTA-free [Roche] per 50 ml) and lysed by bead disruption. For denaturing lysis, 500 µl SDS lysis buffer (10 mM sodium phosphate, pH 7.0, 1% SDS, 1 mM DTT, 1 mM EDTA, 50 mM NaF, 100 µM sodium orthovanadate, 1 mM PMSF, and 4 µg/ml leupeptin) was added, and the sample was incubated at 95°C for 2 min, and lysate was extracted with 800 µl NP-40 buffer and transferred to a clean tube. For native lysis, the lysate was extracted with 500 µl NP-40 buffer and again with 800 µl and then transferred to a clean tube. Extractions were followed by two clearing spins of 5 and 30 min. Proteins were immunoprecipitated from native protein lysates using an excess of antibody (listed below) and rocking at 4°C for 1 h, followed by addition of Protein A or G Sepharose beads (GE Healthcare), as appropriate, and rocking at 4°C for 30 min. Samples were washed four times with NP-40 buffer. Antibodies: 0.8 µg anti-GFP (Roche), 2 µg anti-FLAG (Sigma-Aldrich), 3 µl rabbit anti-Sid4 antiserum, or 2 µl rabbit anti-Dma1 serum.

Antisera were raised against recombinant GST-mNG or GST-Dma1 (Cocalico), and their specificity was verified by immunoblotting (Figure 2 and Supplemental Figure S4E, respectively). The anti-Dma1 serum was further purified by ammonium sulfate precipitation. The serum was cleared by centrifugation and then precipitated with 0.5 volumes of saturated ammonium sulfate added dropwise and incubated overnight at 4°C. The precipitate was cleared from the serum by centrifugation and then the serum was precipitated with an additional 0.5 volumes of saturated ammonium sulfate added dropwise and incubated overnight at 4°C. The precipitate was pelleted by centrifugation, resuspended in 0.4 volumes phosphate-buffered saline (PBS), and dialyzed three times in PBS.

For lambda phosphatase treatment, immunoprecipitated protein was washed twice with 25 mM HEPES-NaOH (pH 7.4) and 150 mM NaCl and then treated with lambda phosphatase (New England Biolabs) in 1x NEBuffer for PMP and 1 mM $MnCl_2$ and incubated at 30°C for 30–60 min with agitation.

For immunoblotting, proteins were resolved by PAGE (see below), transferred to a polyvinylidene difluoride membrane (Immobilon FL; EMD Millipore), blocked with Odyssey Blocking Buffer (LI-COR Biosciences), and incubated with primary antibody at 2 µg/ml or 1:5000 anti-Dma1 serum or 1:2000 anti-Sid4 serum overnight at 4°C. Primary antibodies were detected with secondary antibodies coupled to IRDye680 or IRDye800 (LI-COR Biosciences, Lincoln, NE) and visualized using an Odyssey Infrared Imaging System (LI-COR Biosciences). Resolving gels: 3–8% Tris-acetate PAGE used for Dma1-FLAG and Sid4-DUB blotting; 4–12% NuPAGE used for Dma1-GFP, Sid4, and Dma1 ubiquitination assay blotting, 12% Tris-glycine PAGE used for Cdc2 blotting.

ACKNOWLEDGMENTS

We thank Ilektra Kouranti and Tyler McKann for contributing to the cDNA cloning of DUBs used in this study, Anna Feoktistova and Liping Ren for outstanding technical support, Maya Igarashi for technical contributions, Quanwen Jin for GBP plasmids, and Colin Gordon for DUB plasmids. We are grateful to Rodrigo Guillen, MariaSanta Mangione, Chloe Snider, and Alaina Willet for critical comments on the manuscript. C.M.J. and A.E.J. were supported by the Cellular, Biochemical and Molecular Sciences Training Program (National Institutes of Health [NIH] T32GM08554). Z.C.E. and S.N.C. were supported by the Integrated Biological Systems Training in Oncology Program (2T32CA119925). This work was supported by NIH GM112989 to K.L.G.

REFERENCES

Bahler J, Wu JQ, Longtine MS, Shah NG, McKenzie A 3rd, Steever AB, Wach A, Philippsen P, Pringle JR (1998). Heterologous modules for efficient and versatile PCR-based gene targeting in *Schizosaccharomycespombe*. Yeast 14, 943–951.

Beckley JR, Chen JS, Yang Y, Peng J, Gould KL (2015). A degenerate cohort of yeast membrane trafficking DUBs mediates cell polarity and survival. Mol Cell Proteomics 14, 3132–3141.

Brooks L 3rd, Heimsath EG Jr, Loring GL, Brenner C (2008). FHA-RING ubiquitin ligases in cell division cycle control. Cell Mol Life Sci 65, 3458–3466.
Caydasi AK, Pereira G (2012). SPOC alert—when chromosomes get the wrong direction. Exp Cell Res 318, 1421–1427.
Chang L, Gould KL (2000). Sid4p is required to localize components of the septation initiation pathway to the spindle pole body in fission yeast. Proc Natl Acad Sci USA 97, 5249–5254.
Chen YH, Wang GY, Hao HC, Chao CJ, Wang Y, Jin QW (2017). Facile manipulation of protein localization in fission yeast through binding of GFP-binding protein to GFP. J Cell Sci 130, 1003–1015.
Dischinger S, Krapp A, Xie L, Paulson JR, Simanis V (2008). Chemical genetic analysis of the regulatory role of Cdc2p in the S. pombe septation initiation network. J Cell Sci 121, 843–853.
Elmore ZC, Beckley JR, Chen JS, Gould KL (2014). Histone H2B ubiquitination promotes the function of the anaphase-promoting complex/cyclosome in Schizosaccharomyces pombe. G3 (Bethesda) 4, 1529–1538.
Fankhauser C, Marks J, Reymond A, Simanis V (1993). The *S.pombe* cdc16 gene is required both for maintenance of p34cdc2 kinase activity and regulation of septum formation: a link between mitosis and cytokinesis? EMBO J 12, 2697–2704.
Garcia-Cortes JC, McCollum D (2009). Proper timing of cytokinesis is regulated by Schizosaccharomyces pombe Etd1. J Cell Biol 186, 739–753.
Gordon C, McGurk G, Wallace M, Hastie ND (1996). A conditional lethal mutant in the fission yeast 26 S protease subunit mts3+ is defective in metaphase to anaphase transition. J Biol Chem 271, 5704–5711.
Gould KL, Ren L, Feoktistova AS, Jennings JL, Link AJ (2004). Tandem affinity purification and identification of protein complex components. Methods 33, 239–244.
Guertin DA, Chang L, Irshad F, Gould KL, McCollum D (2000). The role of the sid1p kinase and cdc14p in regulating the onset of cytokinesis in fission yeast. EMBO J 19, 1803–1815.
Guertin DA, Venkatram S, Gould KL, McCollum D (2002). Dma1 prevents mitotic exit and cytokinesis by inhibiting the septation initiation network (SIN). Dev Cell 3, 779–790.
Hagan I, Yanagida M (1995). The product of the spindle formation gene sad1+ associates with the fission yeast spindle pole body and is essential for viability. J Cell Biol 129, 1033–1047.
Hagan IM, Hyams JS (1988). The use of cell division cycle mutants to investigate the control of microtubule distribution in the fission yeast Schizosaccharomyces pombe. J Cell Sci 89, 343–357.
He X, Patterson TE, Sazer S (1997). The Schizosaccharomyces pombe spindle checkpoint protein mad2p blocks anaphase and genetically interacts with the anaphase-promoting complex. Proc Natl Acad Sci USA 94, 7965–7970.
Hiraoka Y, Toda T, Yanagida M (1984). The NDA3 gene of fission yeast encodes beta-tubulin: a cold-sensitive nda3 mutation reversibly blocks spindle formation and chromosome movement in mitosis. Cell 39, 349–358.
Johnson AE, Chen JS, Gould KL (2013). CK1 is required for a mitotic checkpoint that delays cytokinesis. Curr Biol 23, 1920–1926.
Johnson AE, Collier SE, Ohi MD, Gould KL (2012a). Fission yeast Dma1 requires RING domain dimerization for its ubiquitin ligase activity and mitotic checkpoint function. J Biol Chem 287, 25741–25748.
Johnson AE, Gould KL (2011). Dma1 ubiquitinates the SIN scaffold, Sid4, to impede the mitotic localization of Plo1 kinase. EMBO J 30, 341–354.
Johnson AE, McCollum D, Gould KL (2012b). Polar opposites: fine-tuning cytokinesis through SIN asymmetry. Cytoskeleton (Hoboken) 69, 686–699.
Kang D, Chen J, Wong J, Fang G (2002). The checkpoint protein Chfr is a ligase that ubiquitinates Plk1 and inhibits Cdc2 at the G2 to M transition. J Cell Biol 156, 249–259.
Koch A, Krug K, Pengelley S, Macek B, Hauf S (2011). Mitotic substrates of the kinase aurora with roles in chromatin regulation identified through quantitative phosphoproteomics of fission yeast. Sci Signal 4, rs6.
Komander D, Reyes-Turcu F, Licchesi JD, Odenwaelder P, Wilkinson KD, Barford D (2009). Molecular discrimination of structurally equivalent Lys 63-linked and linear polyubiquitin chains. EMBO Rep 10, 466–473.
Kouranti I, McLean JR, Feoktistova A, Liang P, Johnson AE, Roberts-Galbraith RH, Gould KL (2010). A global census of fission yeast deubiquitinating enzyme localization and interaction networks reveals distinct compartmentalization profiles and overlapping functions in endocytosis and polarity. PLoS Biol 8, e1000471.
Krapp A, Collin P, Cano Del Rosario E, Simanis V (2008). Homoeostasis between the GTPase Spg1p and its GAP in the regulation of cytokinesis in S. pombe. J Cell Sci 121, 601–608.
Krapp A, Simanis V (2008). An overview of the fission yeast septation initiation network (SIN). Biochem Soc Trans 36, 411–415.
Lok GT, Sy SM, Dong SS, Ching YP, Tsao SW, Thomson TM, Huen MS (2012). Differential regulation of RNF8-mediated Lys48- and Lys63-based poly-ubiquitylation. Nucleic Acids Res 40, 196–205.
Ma ZQ, Dasari S, Chambers MC, Litton MD, Sobecki SM, Zimmerman LJ, Halvey PJ, Schilling B, Drake PM, Gibson BW, Tabb DL (2009). IDPicker 2.0: Improved protein assembly with high discrimination peptide identification filtering. J Proteome Res 8, 3872–3881.
Marks J, Fankhauser C, Simanis V (1992). Genetic interactions in the control of septation in *Schizosaccharomycespombe*. J Cell Sci 101, 801–808.
McDonald WH, Ohi R, Miyamoto DT, Mitchison TJ, Yates JR III (2002). Comparison of three directly coupled HPLC MS/MS strategies for identification of proteins from complex mixtures: single-dimension LC-MS/MS, 2-phase MudPIT, and 3-phase MudPIT. Int J Mass Spectrom 219, 245–251.
McLean JR, Kouranti I, Gould KL (2011). Survey of the phosphorylation status of the Schizosaccharomyces pombe deubiquitinating enzyme (DUB) family. J Proteome Res 10, 1208–1215.
Mendoza M, Barral Y (2008). Co-ordination of cytokinesis with chromosome segregation. Biochem Soc Trans 36, 387–390.
Moreno S, Klar A, Nurse P (1991). Molecular genetic analysis of fission yeast *Schizosaccharomycespombe*. Methods Enzymol. 194, 795–823.
Morrell JL, Tomlin GC, Rajagopalan S, Venkatram S, Feoktistova AS, Tasto JJ, Mehta S, Jennings JL, Link A, Balasubramanian MK, Gould KL (2004). Sid4p-Cdc11p assembles the septation initiation network and its regulators at the S. pombe SPB. Curr Biol 14, 579–584.
Mulvihill DP, Petersen J, Ohkura H, Glover DM, Hagan IM (1999). Plo1 kinase recruitment to the spindle pole body and its role in cell division in *Schizosaccharomycespombe*. Mol Biol Cell 10, 2771–2785.
Murone M, Simanis V (1996). The fission yeast dma1 gene is a component of the spindle assembly checkpoint, required to prevent septum formation and premature exit from mitosis if spindle function is compromised. EMBO J 15, 6605–6616.
Musacchio A (2015). The molecular biology of spindle assembly checkpoint signaling dynamics. Curr Biol 25, R1002–1018.
Nahse V, Christ L, Stenmark H, Campsteijn C (2017). The abscission checkpoint: making it to the final cut. Trends Cell Biol 27, 1–11.
Ohkura H, Hagan IM, Glover DM (1995). The conserved *Schizosaccharomycespombe* kinase plo1, required to form a bipolar spindle, the actin ring, and septum, can drive septum formation in G1 and G2 cells. Genes Dev 9, 1059–1073.
Rincon SA, Paoletti A (2012). Mid1/anillin and the spatial regulation of cytokinesis in fission yeast. Cytoskeleton (Hoboken) 69, 764–777.
Roberts-Galbraith RH, Chen JS, Wang J, Gould KL (2009). The SH3 domains of two PCH family members cooperate in assembly of the Schizosaccharomyces pombe contractile ring. J Cell Biol 184, 113–127.
Rosenberg JA, Tomlin GC, McDonald WH, Snydsman BE, Muller EG, Yates JR 3rd, Gould KL (2006). Ppc89 links multiple proteins, including the septation initiation network, to the core of the fission yeast spindle-pole body. Mol Biol Cell 17, 3793–3805.
Rothbauer U, Zolghadr K, Muyldermans S, Schepers A, Cardoso MC, Leonhardt H (2008). A versatile nanotrap for biochemical and functional studies with fluorescent fusion proteins. Mol Cell Proteomics 7, 282–289.
Rothbauer U, Zolghadr K, Tillib S, Nowak D, Schermelleh L, Gahl A, Backmann N, Conrath K, Muyldermans S, Cardoso MC, Leonhardt H (2006). Targeting and tracing antigens in live cells with fluorescent nanobodies. Nat Methods 3, 887–889.
Shaner NC, Lambert GG, Chammas A, Ni Y, Cranfill PJ, Baird MA, Sell BR, Allen JR, Day RN, Israelsson M, *et al*. (2013). A bright monomeric green fluorescent protein derived from Branchiostoma lanceolatum. Nat Methods 10, 407–409.
Simanis V (2015). Pombe's thirteen—control of fission yeast cell division by the septation initiation network. J Cell Sci 128, 1465–1474.
Stone M, Hartmann-Petersen R, Seeger M, Bech-Otschir D, Wallace M, Gordon C (2004). Uch2/Uch37 is the major deubiquitinating enzyme

associated with the 26S proteasome in fission yeast. J Mol Biol 344, 697–706.
Stringer DK, Piper RC (2011). Terminating protein ubiquitination: Hasta la vista, ubiquitin. Cell Cycle 10, 3067–3071.
Tabb DL, Fernando CG, Chambers MC (2007). MyriMatch: highly accurate tandem mass spectral peptide identification by multivariate hypergeometric analysis. J Proteome Res 6, 654–661.
Tagwerker C, Flick K, Cui M, Guerrero C, Dou Y, Auer B, Baldi P, Huang L, Kaiser P (2006). A tandem affinity tag for two-step purification under fully denaturing conditions: application in ubiquitin profiling and protein complex identification combined with in vivocross-linking. Mol Cell Proteomics 5, 737–748.
Tanaka K, Petersen J, MacIver F, Mulvihill DP, Glover DM, Hagan IM (2001). The role of Plo1 kinase in mitotic commitment and septation in *Schizosaccharomycespombe*. EMBO J 20, 1259–1270.
Vora SM, Phillips BT (2016). The benefits of local depletion: The centrosome as a scaffold for ubiquitin-proteasome-mediated degradation. Cell Cycle 15, 2124–2134.
Wach A, Brachat A, Poehlmann R, Philippsen P (1994). New heterologous modules for classical or PCR-based gene disruptions in Saccharomyces cerevisiae. Yeast 10, 1793–1808.
Wang Y, Li WZ, Johnson AE, Luo ZQ, Sun XL, Feoktistova A, McDonald WH, McLeod I, Yates JR 3rd, Gould KL, *et al*. (2012). Dnt1 acts as a mitotic inhibitor of the spindle checkpoint protein dma1 in fission yeast. Mol Biol Cell 23, 3348–3356.
Waters JC (2009). Accuracy and precision in quantitative fluorescence microscopy. J Cell Biol 185, 1135–1148.
Willet AH, McDonald NA, Bohnert KA, Baird MA, Allen JR, Davidson MW, Gould KL (2015). The F-BAR Cdc15 promotes contractile ring formation through the direct recruitment of the formin Cdc12. J Cell Biol 208, 391–399.